JJEE
Volume X | Number X | Month 20XX | Pages XXX-XXX

Jordan Journal of Electrical Engineering

ISSN (print): 2409-9600, ISSN (online): 2409-9619

Homepage: jjee.ttu.edu.jo

An Intelligence-Based Controller for Improved Frequency Regulation in Deregulated Power Environment

Rakesh Kumar Singh[1*], Vimlesh Verma[2]

[1, 2] Electrical Engineering Department, National Institute of Technology Patna, Patna, India
E-mail: rakeshsingh8486@gmail.com

Received: Jul 10, 2023 *Revised: Oct 07, 2023* *Accepted: Oct 17, 2023* *Available online: Jun 2, 2024*

***Abstract*—** A methodology for designing and assessing an optimal controller to regulate frequency in a two-area interconnected power system with Renewable Energy Sources (RES) is demonstrated in this paper. The Load Frequency Control (LFC) system makes it possible to restore both system frequency and scheduled tie-line power to their nominal values in a deregulated environment. The introduction of an advanced controller has the potential to improve the LFC mechanism's performance. The present article employs the Inertia Emulation Technique (IET) to demonstrate the potential influence of the novel High Voltage Direct Current (HVDC) tie-line model and converter capacitors. The Integral Time-weighted Absolute Error (ITAE) has been taken as an objective function for the proposed controller. This investigation proposes a novel adaptive control strategy i.e., ANN-based ($PI^{\lambda f}$ + $PI^{\lambda}DN$) controller for the anticipated LFC mechanism. The modified Quasi-Opposition-learning-based Volleyball Premier League (QOVPL) method is utilized to assess the optimal control parameters with the highest efficacy. The effectiveness of the proposed LFC framework has been evaluated through the implementation of established methodologies for managing step and random load perturbations. The supremacy and effectiveness of the proposed control scheme are validated over recently published work.

***Keywords*—** High voltage direct current; Load frequency control; Artificial neural network; Inertia emulation technique; Quasi-opposition-learning-based volleyball premier league.

Nomenclature

LFC	Load Frequency Control	PIDN	Proportional-Integral-Derivative with derivative N-filter
ACE	Area Control Error	QOVPL	Quasi-Opposition-learning-based Volleyball Premier League
AGC	Automatic Generation Control	RES	Renewable Energy Sources
ANN	Artificial Neural Network	VPL	Volleyball Premier League
DB	Dead Band	WOA	Whale Optimization Algorithm
DISCO	Distribution Company	K_P	Proportional constant
DPM	DISCO Participation Matrix	K_I	Integral constant
GENCO	Generation Company	K_D	Derivative constant
GRC	Generation Rate Constraint	λ	Order of an integrator.
HVDC	High Voltage Direct Current	λf	Integrator's non-integer order
IAE	Integral Absolute Error	cpf	contract participation factor
IET	Inertia Emulation Technique	ij	Area number
ISE	Integral Squared Error	T_R, T_{RH}	Transient droop
ITAE	Integral Time-weighted Absolute Error	K_{PSi}	Power system gain
ITSE	Integral Time-weighted Squared Error	T_{ti}	Thermal turbine constant
PI	Proportional-Integral	T_{Gi}	Thermal governor time constant

* Corresponding author
DOI: https://doi.org/10.5455/jjee.204-1688991644

1. INTRODUCTION

The modern electrical power system is made up of multiple interconnected generating power units. An imbalance between total generation and load demand, and other variables can all lead to inefficient power system operations. Implementing load frequency control is a possible solution to the difficult problem of maintaining the specified magnitudes of system frequency and tie-line power under regular and irregular operational conditions. The aforementioned issue poses a considerable challenge in the context of LFC [1, 2], for which a clear-cut resolution is currently unavailable.

Over the past few decades, there have been numerous research papers regarding the LFC of unified power systems, which are responsible for providing electricity to multiple locations. Ranjan et al. provide a short and brief explanation of the LFC's objectives and goals [3]. A study comparing numerous classical controllers operating in a distributed, thermal, and hydrothermal network was published, and the author was later discovered through field research [4-7].

FODs of optimization techniques are demonstrated by comparing them to some contemporary optimization methods using a modified OSHO (Opposition-based Sea-Horse Optimization) methodology [8]. In the article [9], the PID controller was employed to analyze LFC. To improve frequency deviations in hybrid renewable power systems, a robust PID controller has been developed [10].

In the article [11], the modified TID controller was employed to analyze LFC. Arya Y. [12] to regulate the frequency utilized the implementation of a state-of-the-art fuzzy fractional-order (FOPI-FOPDN) controller. The use of a TDF-TIDF controller led to an enhancement in the load frequency controller's performance [13]. The controller coefficients are adaptively tuned using a quasi-oppositional Harris Hawks optimization [14]. Studies on LFC have employed using hPSO-MSC Algorithm, and FO-hPID-fuzzy PID controllers [15]. The use of the Quasi-Opposition Reptile Search Algorithm (QORSA) technique to optimize the FID-T controller on a multi-area network is discussed [16]. The papers [17–20] analyzed the concept of LFC by implementing a power system that combined conventional and renewable energy sources. A study was conducted [21, 22] to develop a Fuzzy Logic based controller. The previously mentioned survey is summarized in Table 1.

The proposed controller i.e., ANN-based ($PI^{\lambda f}$ + $PI^{\lambda}DN$) is studied for deregulated two-area multi-source thermal-hydro-gas power system. In addition, various case studies are used to examine the performance of an IET-based High Voltage Direct Current (HVDC) interconnected power system. From the above discussion, the following are the main contributions of the studied system:

a) Thermal-hydro-gas power structure has been designed for a deregulated power environment.
b) IET-based modified HVDC power structure is designed to incorporate Renewable Energy Sources (RES).
c) ANN-based ($PI^{\lambda f}$ + $PI^{\lambda}DN$) controller has been designed and tested for the proposed LFC system.
d) A modified QOVPL has been implemented for getting different optimized gains of the system.
e) The proposed LFC has been validated through improved results analysis, robustness analysis, and with existing recent work of literature.

Table 1. Summary of the survey revealing AGC's work.

Ref.	Algorithm	Controller	Deregulation	Nonlinearity	Energy Storage Systems	Generating Units
[12]	ICA	Fuzzy FOPI-FOPDN	No	None	None	3-area thermal
[14]	QOHHO	Two-DOF FFO-PI-TD	Yes	GDB, GRC, BD	ESS	Thermal, Biogas, PTST, Wind
[15]	hPSO-MSC Algorithm	FO-hPID-Fuzzy PID	No	GRC	None	3-area thermal
[16]	QORSA	FID-T	No	GDB, GRC, BD	EV	Thermal, Hydro, Gas, RES
[17]	OVPL Algorithm	Intelligent Fuzzy-FOPI	Yes	GDB, GRC, BD	IET	Thermal, Hydro, Gas, DG
[19]	QOAEF Algorithm	Fuzzy FOPI-LADRC	Yes	BD, GRC	BESS, EV	Thermal, Biogas, DG
This Work	QOVPL Algorithm	ANN-based (PIλf + PIλDN)	Yes	GRC	IET	Thermal, Hydro, Gas, RES

2. THE INVESTIGATED SYSTEM

2.1. Modeling of the Experimental Systems

This article investigates the feasibility of establishing a thermal-hydro-gas power plant that would supply electricity to two distinct areas in a deregulated energy market. Area 2 can produce twice as much energy as Area 1 (4,000 megawatts). Area 1 has a capacity of 2,000 MW.

Each area contains four companies: two-generation companies (GENCOs) and two distribution companies (DISCOs).

The thermal power system is the primary GENCO for both (GENCO 1 and 3). Hydroelectricity (GENCO 4) and gas-powered turbines (GENCO 2) power the first two areas. The ISO (Independent System Operator) establishes contracts or linkages between GENCOs and DISCOs through a bidding process.

This is accomplished via competitive bidding procedures. Each of these locations is connected to the others via a parallel AC-HVDC tie-line system. The schematic structure of the described system is depicted in Fig. 1 [23].

Two mathematical models of the interconnection system and individual GENCOs are depicted in Fig. 2 [23] and Fig. 3, respectively, to help illustrate how the concepts in this article function. Generation Rate Constraint (GRC) non-linearity, which restricts the rate at which energy is produced, is increasingly used in thermal power systems.

To maintain stability over time, an ANN-based ($PI^{\lambda f}$ + $PI^{\lambda}DN$) controller is deployed. To further explore their significant impact on the dynamic behavior of the system, simulation research utilizing a modified IET-based High Voltage Direct Current (HVDC) tie-line model is being considered.

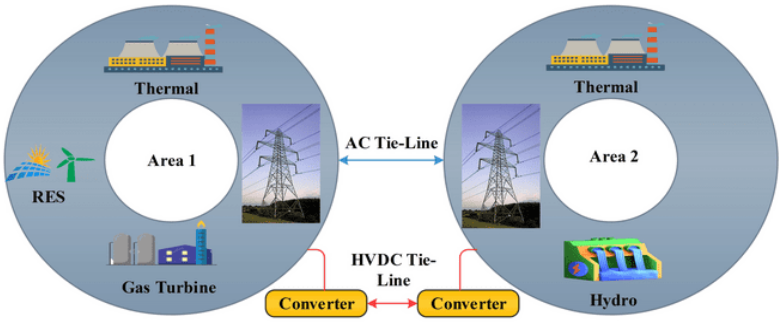

Fig. 1. The two-area interconnected power system.

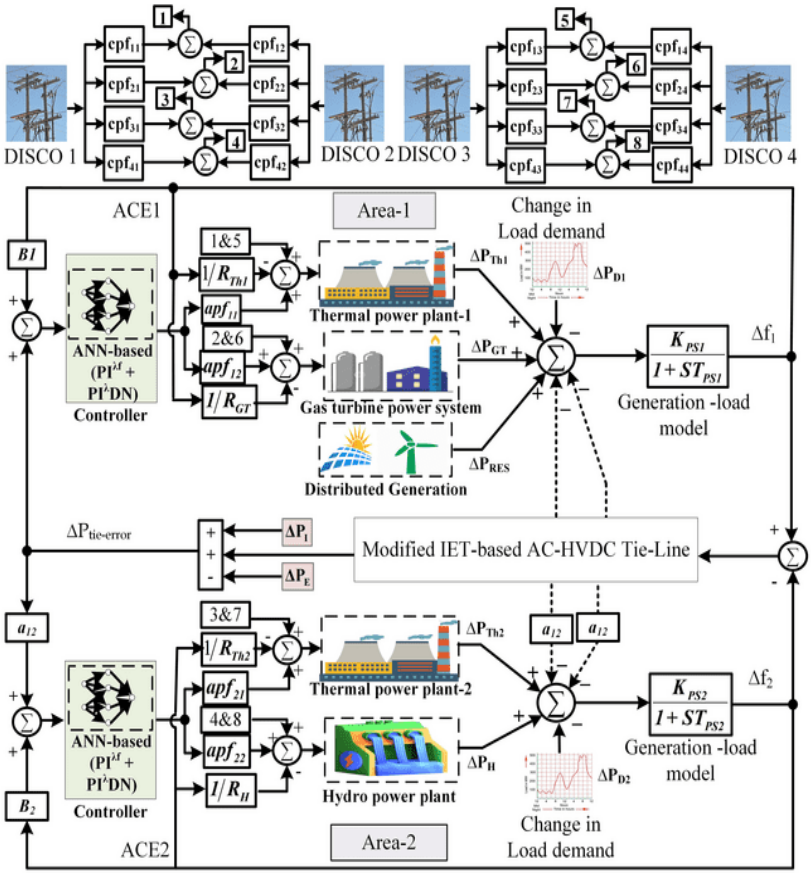

Fig. 2. Schematic test setup for simulation work.

2.2. Objective Function and Performance Index

When there is a mismatch between generated and consumed active power, the governor cannot solely regulate frequency and tie-line power exchange. It establishes a new balance point at the generation level to correct the power imbalance, and a secondary LFC controller restores tie-line power and frequency. The QOVPL algorithm improves the LFC's effectiveness by changing the strategy's control settings. These Objective Functions' (OF) values are shown in Table 2, and the optimization process uses them to choose the best controller settings.

$$\left.\begin{aligned} OF_{IAE} &= \int_0^t \left(\sum|\Delta f_i| + \sum|\Delta P_{tie,ij}|\right)dt \\ OF_{ISE} &= \int_0^t \left(\sum\Delta f_i^2 + \sum\Delta P_{tie,ij}^2\right)dt \\ OF_{ITAE} &= \int_0^t \left(\sum|\Delta f_i| + \sum|\Delta P_{tie,ij}|\right) \times t_s dt \\ OF_{ITSE} &= \int_0^t \left(\sum\Delta f_i^2 + \sum\Delta P_{tie,ij}^2\right) \times t_s dt \end{aligned}\right\} \quad (1)$$

where i and j are the area numbers.

Table 2. Calculation of the system's response to a step-change in load demand.

Controllers		Δf_1			Δf_2			ΔP_{12}			OF
		OS	US (-ve)	TS	OS	US (-ve)	TS	OS	US (-ve)	TS	
FOPI		0.056	0.054	99.4	0.028	0.0283	99.57	0.013	0.01280	99.96	4.50
Fuzzy FOPI		0.025	0.027	99.6	0.009	0.0200	99.96	0.005	0.00880	99.93	1.12
ANN-tuned PIDN		0.000	0.011	12.9	0.039	0.0064	13.81	0.000	0.00294	32.68	7.01×10^{-2}
Fuzzy (PIʎ)+PIʎDN		0.004	0.014	6.07	0.003	0.0095	6.354	0.000	0.00320	6.707	9.49×10^{-5}
ANN-based PIʎDN		0.000	0.012	8.15	0.027	0.0067	11.20	0.000	0.00313	96.84	6.35×10^{-2}
Proposed controller	IAE	0.000	0.012	15.1	0.000	0.0080	20.95	0.000	0.00313	48.32	7.05×10^{-2}
	ISE	0.009	0.004	21.3	0.000	0.0028	24.38	0.000	0.00110	49.95	4.25×10^{-2}
	ITAE	0.001	0.013	11.8	0.002	0.0102	16.10	0.000	0.00442	48.37	0.6077
	ITSE	0.000	0.012	8.10	0.027	0.0066	11.02	0.000	0.00122	46.39	6.11×10^{-2}

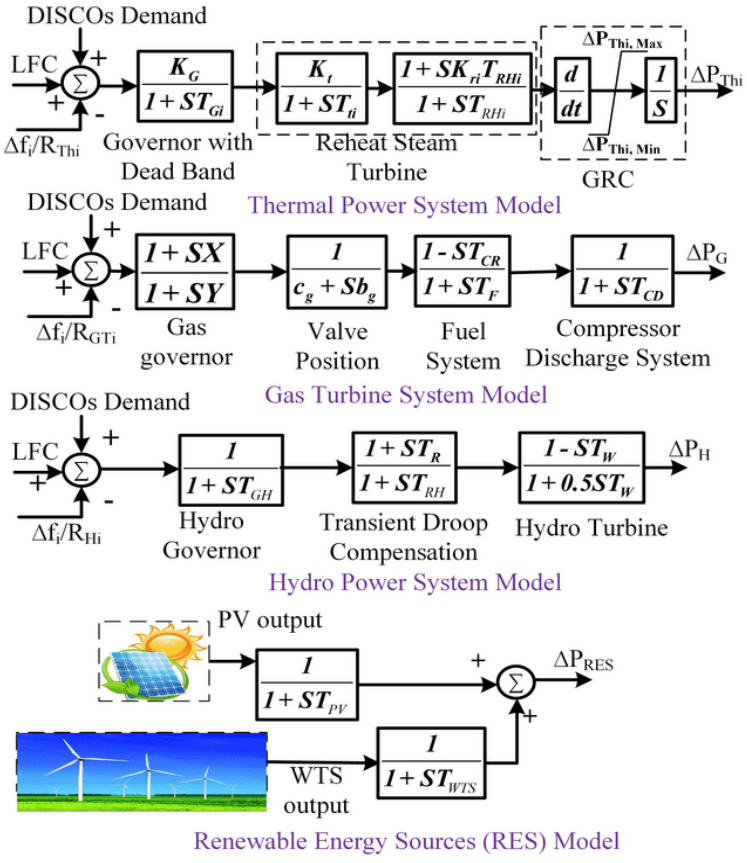

Fig. 3. Model with transfer function inputs and outputs.

3. MODELING OF IET-BASED AC-HVDC TIE-LINE

3.1. IET-based Model Analysis of the AC-HVDC Tie-Line

Parallel AC-HVDC transmission line topologies have increased in use during the past few decades. This approach enhances transfer capacity while minimizing losses. This is a

significant advancement because a nominal tie-line power exchange is the primary objective of the LFC study. Parallel AC-HVDC tie-lines affected LFC. The numerical expressions and parameter computations of the model are not available. Due to this, investigates an accurate HVDC model using the appropriate mathematical notation. The process used to create AC-HVDC models using the IET is the same as this one. The procedure for building an AC-HVDC tie line includes the establishment of the synchronization coefficients.

3.2. Calculation of the Corresponding Tie-Line Synchronization Coefficients

The test system delineates two distinct capacity areas, one with a capacity of 2000 MW and the other with a capacity of 4000 MW. The ends of the parallel AC-HVDC tie-line system is depicted in Fig. 1. The AC and HVDC (High Voltage Direct Current) tie-lines may each transfer up to 200 MW and 600 MW of power, respectively, according to the authors' assumptions in this analysis.

The voltage sources $E_1\angle\theta_1$ and $E_2\angle\theta_2$ in series with the reactance's X_1 and X_2 are an illustration of the High Voltage Direct Current (HVDC) power electronic converters. $V_1\angle\theta_1$ and $V_2\angle\theta_2$ denote the corresponding bus voltages for the first and second areas, respectively. An electrical equivalent circuit with these parts is shown in Fig. 4. Linearize power flow over AC and HVDC tie-lines by utilizing Eqs. (2) and (3).

$$\Delta P_{tie,AC} = \frac{2\pi T_{tie,AC}}{s}(\Delta f_1 - \Delta f_2) \tag{2}$$

$$\Delta P_{tie,DC} = \frac{2\pi T_{tie,DC}}{s}(\Delta f_1 - \Delta f_2) \tag{3}$$

where the AC tie-line synchronization coefficient is $T_{tie,AC}$ and the HVDC tie-line synchronization coefficient is $T_{tie,DC}$.

$$T_{tie,AC} = \frac{P_{AC,max}}{P_{rated}}\cos(\delta_1 - \delta_2) \tag{4}$$

$$T_{\text{tie},DC} = \frac{T_{DC1} \times T_{DC2}}{T_{DC1} + T_{DC2}} \tag{5}$$

where,

$$T_{DC1} = \frac{P_{DC,max}}{\text{P}_{\text{rated},1}}\cos(\delta_1 - \theta_1), T_{DC2} = \frac{P_{DC,max}}{\text{P}_{ratid,2}}\cos(\delta_2 - \theta_2)$$

Calculating the synchronization coefficient requires assuming that the AC tie-line is 50% loaded.

$$\sin(\delta_1 - \delta_2) = \frac{P_{\text{tie},AC}}{P_{AC,max}} = \frac{100}{200} = 0.5; (\delta_1 - \delta_2) = 30^\circ$$

$$T_{\text{tie},AC} = 0.0867 \tag{6}$$

For example, this is how the coefficient of the 50% loaded HVDC tie-synchronization line was worked out:

$$\sin(\delta_1 - \theta_1) = \sin(\delta_2 - \theta_2) = \frac{P_{tie,DC}}{P_{DC,\text{max}}} = \frac{300}{600} = 0.5$$

Since the reported capacities are equal for both areas,

$T_{DC1} = 0.2598$; $T_{DC2} = 0.1299$

$$T_{tie,DC} = \frac{T_{DC1} \times T_{DC2}}{T_{DC1} + T_{DC2}} = 0.0866 \tag{7}$$

For a wide range of loading scenarios, HVDC tie-line synchronization coefficients can be calculated.

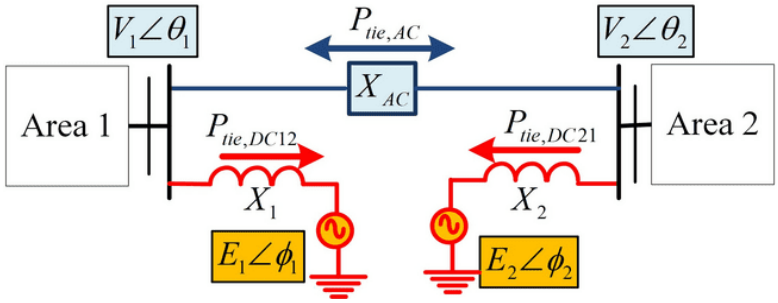

Fig. 4. Schematic diagram of the AC-HVDC tie line.

3.3. Use of the Inertia Emulation Technique (IET) on HVDC Tie Lines

The DC capacitors in the HVDC converters allow for frequency adjustment. This paper describes one such method that can be applied to load frequency control (LFC). It can be demonstrated that the charging equation is for a DC capacitor (C_{DC}) with rated capacity S_{DC} and operational voltage V_{DC}.

$$nC_{DC}V_{DC}^{\circ}\frac{d}{dt}\Delta V_{DC} = P_{in} - P_{\text{out}} = P_{\text{tie, }DC} \tag{8}$$

Here is the linearized expression, Eq. (8), on a per-unit basis:

$$\left(\frac{nC_{DC}}{S_{DC}}\right)V_{DC}^{\circ}\frac{d}{dt}\Delta V_{DC} = \Delta P_{\text{tie},DC} \tag{9}$$

The synchronous machine's swing Eq. (10), rather than the equation for charging a capacitor;

$$\left(\frac{2H}{f_o}\right)\frac{d}{dt}(\Delta f) = \Delta P_m - \Delta P_e = \Delta P_{SM} \tag{10}$$

It is possible to express it in writing by using Eqs. (9) and (10).

$$\left(\frac{nC_{DC}}{S_{DC}}\right)V_{DC}^{\circ}\frac{d}{dt}\Delta V_{DC} = \left(\frac{2H}{f_0}\right)\frac{d}{dt}(\Delta f) \tag{11}$$

Applying the Laplace transformation can be used to derive the formula for the voltage fluctuation provided in Eq. (11).

$$\Delta V_{DC}(s) = \left(\frac{2Hs}{nC_{DC}f_o(V_{DC}^{\circ})^2}\right)\Delta f(s) \tag{12}$$

This equation explains how charging voltage fluctuation and frequency are related. The power-reference signal is produced by multiplying the measured voltage by the tie-line current. The value 'I' can be assigned based on the HVDC tie-load line condition. The value of "I" is set to 0.5 because the loading is 50%. The IET for transferring function simulation is further described in Fig. 5 [23].

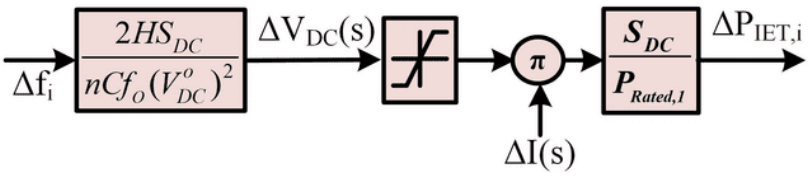

Fig. 5. The IET model for transfer function simulation.

4. DEREGULATION FOR THE PROPOSED LFC

In the deregulated electricity markets of today, ISO uses competitive bidding to figure out how supply and demand are linked. Both GENCO and DISCO will put in bids, and the contracts will be decided by talking to the highest bidders. The parties will conduct LFC investigations using a DISCOs Participation Matrix (DPM). Each DPM entry contains the *cpf*

for the related GECNO contract. There are two GENCOs and two DISCOs in each area for testing. Using the DPM as an example:

$$DPM = \begin{bmatrix} cpf_{11} & cpf_{12} & cpf_{13} & cpf_{14} \\ cpf_{21} & cpf_{22} & cpf_{23} & cpf_{24} \\ cpf_{31} & cpf_{32} & cpf_{33} & cpf_{34} \\ cpf_{41} & cpf_{42} & cpf_{43} & cpf_{44} \end{bmatrix} \quad (13)$$

GENCO rows and DISCO columns make up a DPM. Thus, deliberate transfers of jurisdictional authority are referred to as

$$\Delta P_{\text{tie},sch} = P_E - P_I \quad (14)$$

Electricity exported is equal to electricity exported less electricity imported, or PE minus PI. A different way to say the tie-line is as follows:

$$\Delta P_{\text{tie, error}} = \Delta P_{\text{tie, act}} - \Delta P_{\text{tie, }sch} \quad (15)$$

As a result of this effort's focus on using parallel AC-IET technology for HVDC tie-lines, the actual tie-line power is as follows:

$$\Delta P_{\text{tie, act}} = \left(\Delta P_{\text{tie, DC}} - \Delta P_{\text{IET,1}} - a_{12}\Delta P_{\text{IET, 2}}\right) + \Delta P_{\text{tie, AC}} \quad (16)$$

As a reference for the controllers' input, the following expression, which characterizes the ensuing Area Control Error (ACE), is used:

$$ACE = B_i \Delta f_i + \Delta P_{\text{tie, error}} \quad (17)$$

Bilateral, poolco-based, and hybrid transactions are all considered unrestricted transactions. The nearby PBT power plants adjust to changing demand. All connected GENCOs worked together to create the BBT load-type switch. Combining PBT and BBT types enables a deeper investigation of a variety of scenarios.

5. THE PROPOSED CONTROLLER AND OPTIMIZATION TECHNIQUE

5.1. ANN-based (PIλf + PIλDN) controller

A subset of specialized data-handling networks called artificial neural networks (ANNs) aims to mimic the functionality of biological neural networks. In a normal architecture, the neurons cooperate to carry out their jobs in parallel.

This structure contains neurons at a very high density. 'Connecting links', which are created between two neurons, are used to connect the neurons in an ANN. These interconnected nodes represent the specific information that makes up the input signal by having a known relevance. The only way to address this challenging challenge is to adjust the weight through backpropagation. A closed-loop, ANN-based ($PI^{\lambda f}$ + $PI^{\lambda}DN$) controller is shown in Fig. 6. This is one of its distinctive qualities.

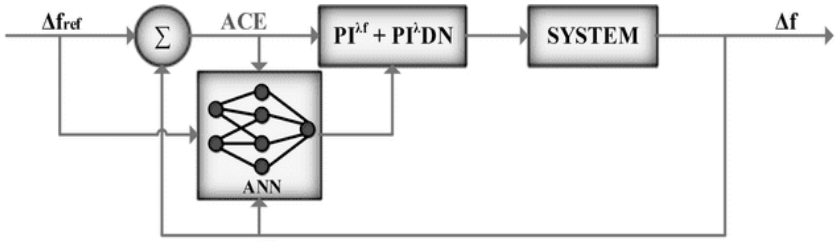

Fig. 6. ANN-based closed-loop ($PI^{\lambda f}$ + $PI^{\lambda}DN$) controller.

Authors strive to reduce their work's error, which can be viewed as a function of the discrepancy between the desired and observed rates of outlier occurrences. The best

(PI$^{\lambda f}$ + PI$^{\lambda}$DN) gains for the system (the ANN's output) can be established by iteratively revising the weights of the connecting connections within the neural network using a backpropagation technique. The key to accomplishing this is a sharp deceleration from high speed. Backpropagation allows the ANN to produce results despite its lack of training. For the controller to learn the parameters of a neural network, the backpropagation technique is used.

5.2. The Backpropagation Algorithm

The (PI$^{\lambda f}$ + PI$^{\lambda}$DN) controller's parameters are optimized using a backpropagation algorithm [24]. Fig. 7 depicts the backpropagation algorithm as a flowchart, which functions as follows:

Step 1. Use *ACE*, Δf, and Δf_{ref} to put the results of the finished model into the ANN (Fig. 2). If the bias input is 1, the device will operate normally. Learning rate coefficients and inertia coefficients must be used to initialize the weights of the hidden layer ($W^{(2)}_{ji}(0)$) and the output layer ($W^{(3)}_{qj}(0)$), respectively.

Step 2. To use $\Delta f(k)$ and Δf_{ref} to derive the efficiency index function $E(k)$. When writing this scenario, authors account for the system's Δf and make Δf_{ref} equal to zero.

Step 3. To do this, the authors figure out the weights $W^{(2)}_{ji}(0)$ and $W^{(3)}_{qj}(0)$ for the output layer and the hidden layer, respectively.

Step 4. The activation function and the most up-to-date weighting factors ($W^{(2)}_{ji}(k)$, $W^{(3)}_{qj}(k)$) are used to calculate the neural network's output. The ANN outputs the parameters of a (PI$^{\lambda f}$ + PI$^{\lambda}$DN) controller with the highest possible efficiency.

Step 5. To verify that the terms of the contract have been fulfilled (number of epochs). Step 2 will be performed with $k = k + 1$ if this requirement is not met.

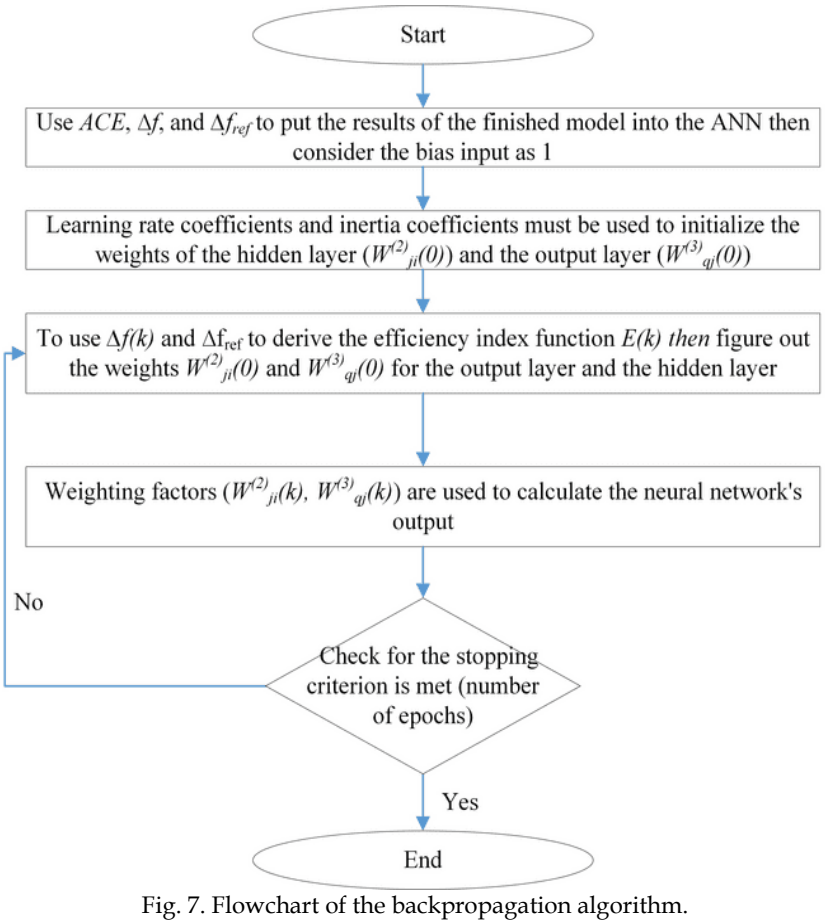

Fig. 7. Flowchart of the backpropagation algorithm.

5.3. The Proposed Adaptive (PIλf + PIλDN) Controller

In the design of controllers, some common configurations include cascading, fractional order, and FLC. Every idea has its benefits and drawbacks. Therefore, the purpose of this article is to outline the collective benefits of certain structures. By incorporating fractional-order and adaptive policy principles. A new controller configuration (i.e., ANN-based ($PI^{\lambda f}$ + $PI^{\lambda}DN$)) has emerged in this paper. The outcomes of some case studies are encouraging. This controller was developed using some of the basic research detailed below.

The common and well-known PID controller is a great way to solve difficult technical problems. Yet because there is a derivative controller, it has noise problems. By including a noise filter and a derivative controller, this is lessened. It is further enhanced by switching out the straightforward integral controller for a fractional-order integrator, which improves the transient response by allowing fractional-order integrator selection. The formula $PI^{\lambda f}$ + $PI^{\lambda}DN$ is as follows:

$$G_{PI^{\lambda f}+\,PI^{\lambda}DN} = K_{Pf} + \frac{K_{If}}{s^{\lambda f}} + K_{P_i} + \frac{K_{I_i}}{s^{\lambda}} + K_{D_i}\frac{sN_i}{s+N_i} \quad (18)$$

where K_{Pf} and K_{If} are proportional and integral gains, respectively, and λf is the integrator's non-integer order. K_{Pi}, K_{Ii}, and K_{Di} are the symbols used to denote the proportional, integral, and derivative gains, respectively. Here, 'i' is the 'i^{th}' area. N is the symbol for the derivative filter constant and λ is the order of an integrator.

For use in LFC investigations, many controllers are available. Notwithstanding their differences, all controllers have benefits and drawbacks. Giving the controllers tuneable weights can also help to extract the best control activity. The addition of the adaptive control method leads to more encouraging outcomes. Fig. 8 depicts the controller structure in detail.

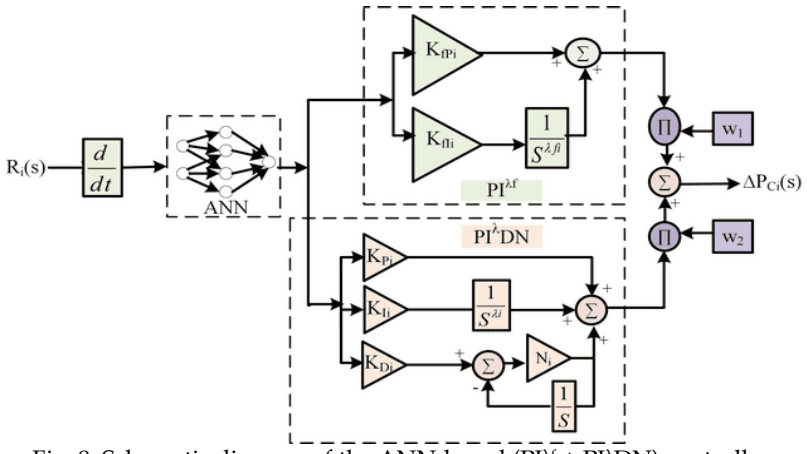

Fig. 8. Schematic diagram of the ANN-based ($PI^{\lambda f}$ + $PI^{\lambda}DN$) controller.

Although there are a few limitations regarding the control approach. This control approach is very complex with neurons and intricate units. These neurons work together with their connections to create a process that is difficult to synchronize in study. The complexity of the system may increase with the implementation of the fractional order control concept.

5.4. The Optimization Technique

Researchers have used a wide range of metaheuristic methods to find the best parameters for the LFC system. When constructing a sturdy and intelligent frequency regulator controller, it is crucial to correctly optimize similar parameters. The authors of this work used the QOVPL (Quasi-Opposition-based Volleyball Premier League) algorithm to optimize the proposed controller.

5.4.1. Volleyball Premier League Algorithm

VPLA surpasses several common algorithms in both exploitation and exploration, making it a potent metaheuristic. This concept was inspired by intense competition and frequent collaboration between volleyball teams. The algorithm also resembles a coach's behavior throughout a game. This motivates the search for volleyball-based metaphors, especially those involving substitution, coaching, and learning. As a starting point for the solution, a random number is employed. The initialized solution, unlike other algorithms, comprises two different components: an active component and a passive component. These two sections reflect the starting line-up and the bench for the volleyball team. If you have two possibilities to choose from rather than one, you may be able to focus your search and arrive at the best solution more quickly.

The schedules of all competing teams follow the same round-robin structure. A game has only two conceivable outcomes: victory and failure. To enhance its standing, the winning team needs only to employ its winning tactics against the league's top three teams. On the other hand, losing teams must incorporate new strategies into their next practice session. In addition, techniques such as replacing underperforming players and spreading tactical information are utilized. Only the top three teams from the previous week may continue utilizing the same strategies the next week. This means that the strategy of the other groups will need to be adjusted accordingly. Following each week, one of the reserve teams replaces the team in last place, and the remaining teams compete to determine who will finish in the top three. VPLA performs admirably and is frequently the best accessible alternative, despite its slowness and tendency to become stuck in the local optimal solution.

5.4.2. Opposition-based Algorithm

There are 2n alternatives produced through opposition-based optimization for each population. The fitness value of all 2n possibilities is used to filter out the top n population and forward it to the next procedural stage. Convergence is enhanced by eliminating earlier solutions with lower fitness ratings [16].

5.4.3. The Proposed Algorithm

The QOVPLA is an upgraded version of the VPLA that incorporates Quasi-Opposition-Based learning principles (QOBL). The VPLA and QOBL have joined forces to address this problem. QOBL is responsible for all revisions to the algorithm's configuration and continuous maintenance. QOBL takes into account the two-way interaction between entities, so it compares the fitness of two solutions for every n-population set. Around fifty percent of the population is removed due to low fitness. Thus, the algorithm's solution time will be highly variable. Fig. 9 depicts the full algorithm (QOVPL) as a flowchart.

6. RESULTS AND DISCUSSION

In addition to outlining the IET's definition of the HVDC tie-line, this article looks into some case studies that make use of the new controller. This setup was made with the help of the MATLAB/Simulink environment and the models described in the last section. Two individual analyses make up the total analysis: Included in the discussion are-

(i) The justification for the Proposed Controller, and the Effect of an IET-based HVDC tie-line on Load Frequency Control (LFC).

(ii) Contract breach, and a review of related literature. In all circumstances, the QOVPL algorithm guarantees the best performance.

6.1 Case Study 1: Justification for the Proposed Controller and the Effect of an IET-based HVDC tie-line on LFC

This case study is based on Section 2's two-area system and the PBT type's unregulated environment. The authors merely need to examine Eq. (19) to get the PBT-DPM that interests them. All GENCOs are anticipated to contribute roughly the same amount to variations in load in their service areas.

$$DPM = \begin{bmatrix} 0.5 & 0.5 & 0 & 0 \\ 0.5 & 0.5 & 0 & 0 \\ 0 & 0 & 0 & 0 \\ 0 & 0 & 0 & 0 \end{bmatrix} \quad (19)$$

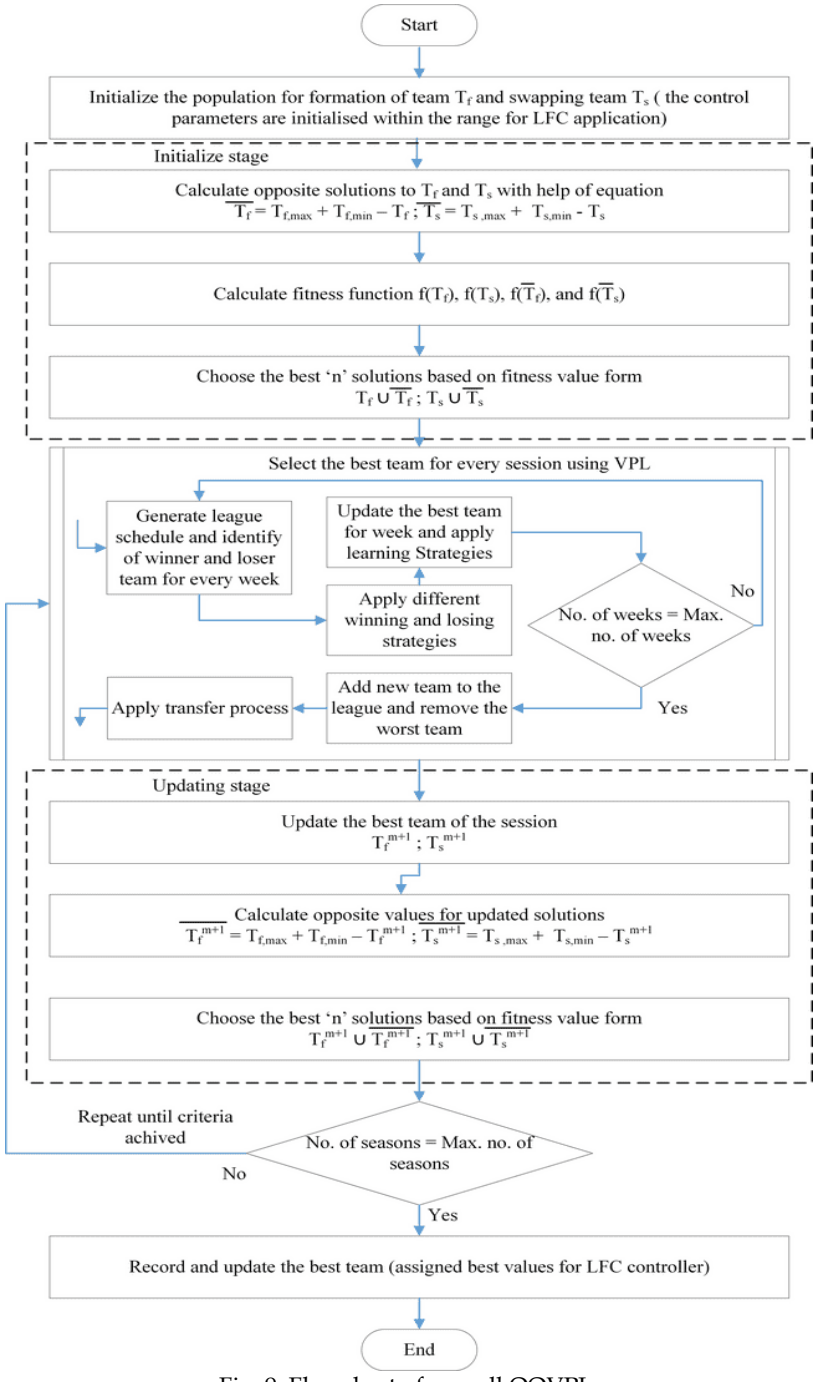

Fig. 9. Flowchart of overall QOVPL.

With the aid of FOPI, Fuzzy FOPI, Fuzzy (PI$^{\lambda f}$) + PI$^{\lambda}$DN, ANN-based PI$^{\lambda}$DN, and the suggested controller with adaptive control, the dynamic performance of the system is captured. According to the QOVPL, Table 3 below lists the control settings for each of the controllers under consideration. Fig. 10 (a), (b), and (c) depict the fluctuations in frequency and tie-line power brought on by the Step-change in Load Demand (SLD).

A plus or minus 5% error margin is used to calculate the settling time. Such proof demonstrates that the suggested controller is successful in generating the required enhanced transient responsiveness. QOVPL performs better than VPL and WOA in terms of error reduction and rise time. Using the values listed in Table 4, Fig. 10(d) shows a plot of an objective function (OF) vs. the number of iterations.

Table 3. QOVPL-determined optimal controller gain values.

Control Parameter	FOPI		Fuzzy FOPI		Fuzzy (PI$^{\lambda}$) + PI$^{\lambda}$DN		ANN-based PI$^{\lambda}$DN		Proposed controller	
	A1	A2	A1	A2	A1	A2	A1	A2	A1	A2
K_{Pi}	0.023	0.184	0.128	0.552	1.256	0.539	0.3875	0.0689	0.3194	0.3763
K_{Ii}	0.123	0.584	0.249	0.110	1.433	0.483	0.1660	0.1237	0.4181	0.6202
K_{Di}	-	-	-	-	1.910	0.910	0.073	0.0044	0.1074	0.0468
K_{Pfi}	-	-	-	-	1.635	1.104	-	-	0.1208	0.0360
K_{Ifi}	-	-	-	-	0.891	1.004	-	-	0.1523	0.0112
N_i	-	-	-	-	61.43	62.38	16.21	24.77	14.012	20.6121
λ_i	0.4890	-	-	-	1.1693	1.1721	1.2184	1.6577	0.1261	0.2310
λ_{fi}	-	0.5817	1.4923	1.2456	0.4204	1.3656	-	-	0.3629	0.1305
K_{1i}	-	-	0.0954	0.1520	0.8595	1.5678	-	-	0.4052	0.0225
K_{2i}	-	-	0.3685	0.0259	0.6268	0.5265	-	-	0.1169	0.4277
w_1	-	-	-	-	1.9103	0.5588	0.0884	0.1104	0.1272	0.1744
w_2	-	-	-	-	0.8468	1.207	0.0167	0.1965	0.3373	0.0767

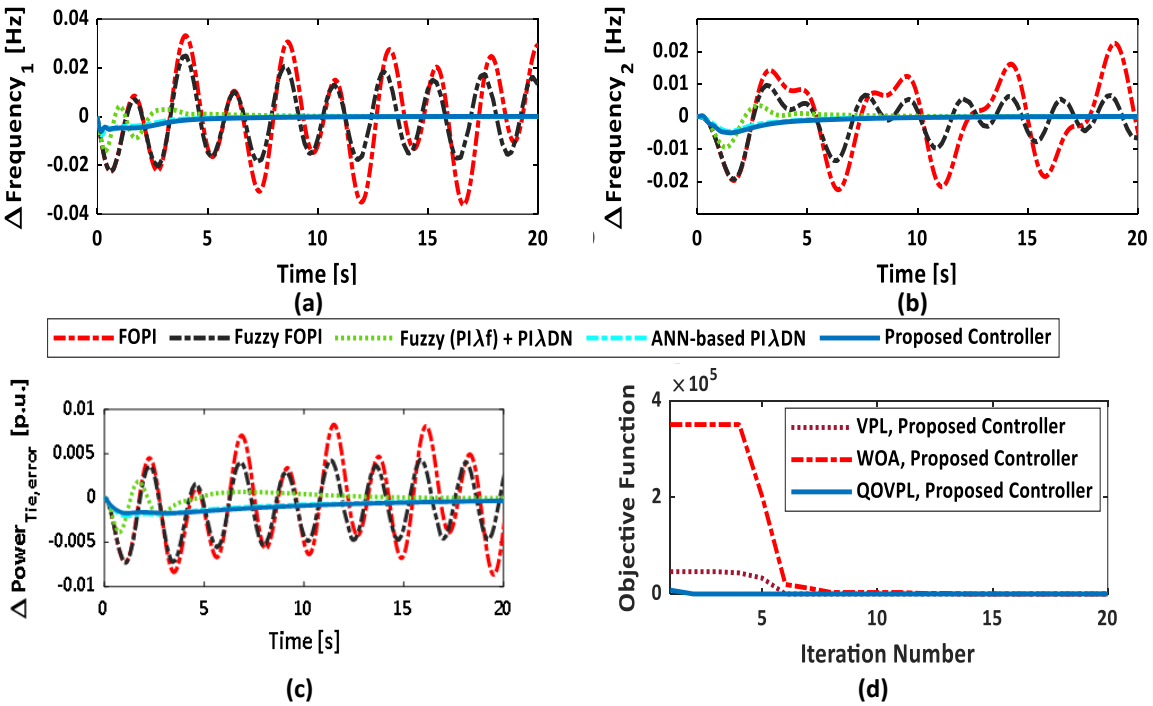

Fig. 10. SLD test system response using different controllers: a) area 1 frequency deviation; b) area 2 frequency deviation; c) tie-line power exchange deviation; d) objective function vs. number of iterations.

Improvements are noticeable when the proposed controller is used in conjunction with adaptive control. A thorough analysis of undershoot, overshoot, and settling time is exhibited in Table 2.

Table 4. Step load-demand algorithms that change the ideal gain values.

Gain	WAO		VPL		QOVPL							
					IAE		ISE		ITAE		ITSE	
	A1	A2	A1	A2	A1	A2	A1	A2	A1	A2	A1	A2
K_{pi}	0.38	0.59	0.76	0.799	0.534	0.442	1.456	0.49	0.491	0.653	0.319	0.376
K_{Ii}	0.69	0.65	0.80	0.891	0.663	0.926	0.667	0.81	0.483	0.592	0.418	0.620
K_{Di}	0.74	0.88	0.76	0.791	0.089	0.674	0.038	0.62	0.023	0.082	0.107	0.046
K_{Pfi}	0.91	0.95	0.88	0.881	0.210	0.903	0.149	0.08	0.138	0.067	0.120	0.036
K_{Ifi}	0.66	0.97	0.65	0.901	0.034	0.283	0.214	0.02	0.176	0.014	0.152	0.011
N_i	61.3	66.3	46.6	58.31	57.10	47.81	52.57	45.6	34.45	27.89	29.01	20.61
λ_i	0.98	0.79	0.56	0.991	1.367	1.221	1.564	1.78	1.349	1.785	0.126	0.231
λ_{fi}	0.89	0.75	0.86	0.530	0.774	0.412	0.735	0.35	0.670	0.267	0.362	0.130
K_{1i}	0.84	0.93	0.79	0.902	0.723	0.059	0.573	0.04	0.546	0.034	0.405	0.022
K_{2i}	0.47	0.94	0.38	0.881	0.299	0.795	0.219	0.71	0.178	0.547	0.116	0.427
w_1	0.49	0.54	0.42	0.083	0.404	0.589	0.974	0.88	0.433	0.134	0.127	0.174
w_2	0.35	0.38	0.23	0.342	0.633	0.832	1.453	0.68	0.281	0.441	0.337	0.076

As a result, ITSE is given more attention as the main optimization goal. The authors of this research concentrate on the PBT variety's deregulation, which has been permitted to experience de-restriction. Due to the load shift only affecting Area 1 (Fig. 11(d)), all GENCOs contributed equally to it. For the case of SLD, the suggested controller with the best parameters found by QOVPL made a big difference. Using the same optimal values from Table 3, the authors looked at how the system handled the chaotic changes in load shown in Fig. 12(a).

Fig. 12 (b), (c), and (d) show how the system reacts to a random load disturbance dynamically. In comparison to the alternatives, the proposed adaptive controller performs better.

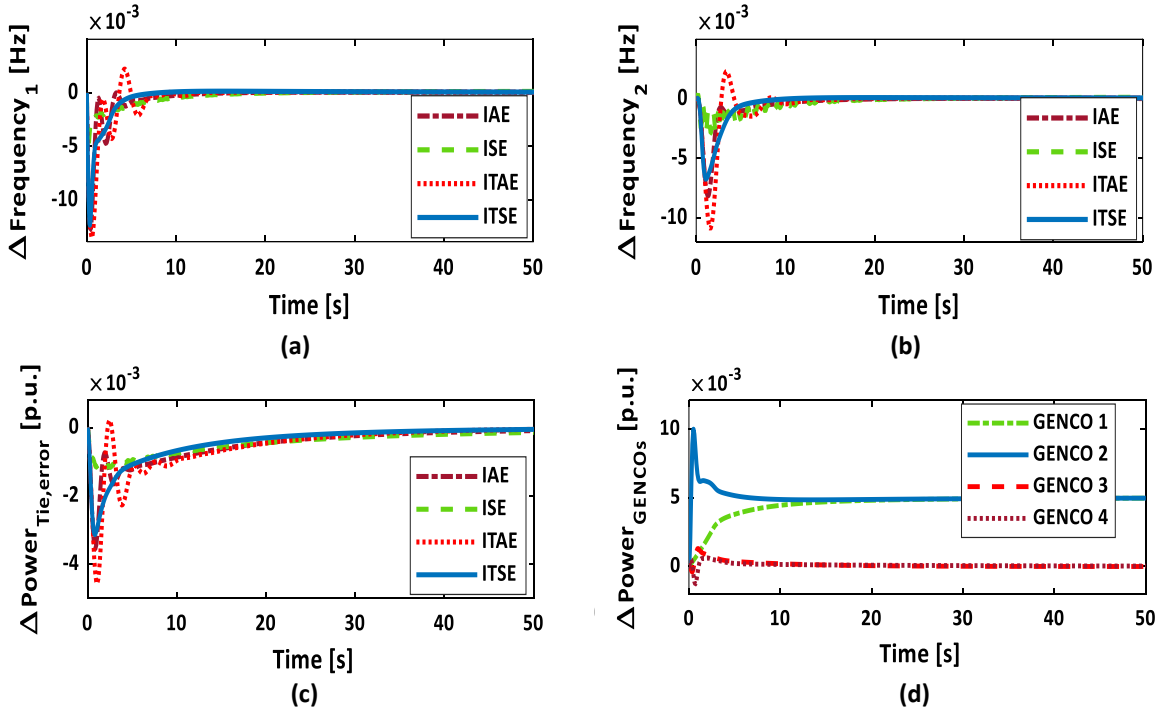

Fig. 11. The test system reaction for four objective functions: a) area 1 frequency deviation; b) area 2frequency deviation; c) tie-line power exchange deviation; d) PBT case GENCO response.

In addition, the four separate categories of objective functions (OF) are IAE, ISE, ITAE, and ITSE (Eq. 1). Figs. 11(a), (b), and (c) demonstrate a system's response using all four OFs. The findings of QOVPL's evaluation of the suggested controller's control settings for different OFs are shown in Table 4.

The numerical findings in Table 2 show how well the suggested controller and system work concerning all OFs. Following the implementation of ITSE, more advancements in OS, US, and TS were noted.

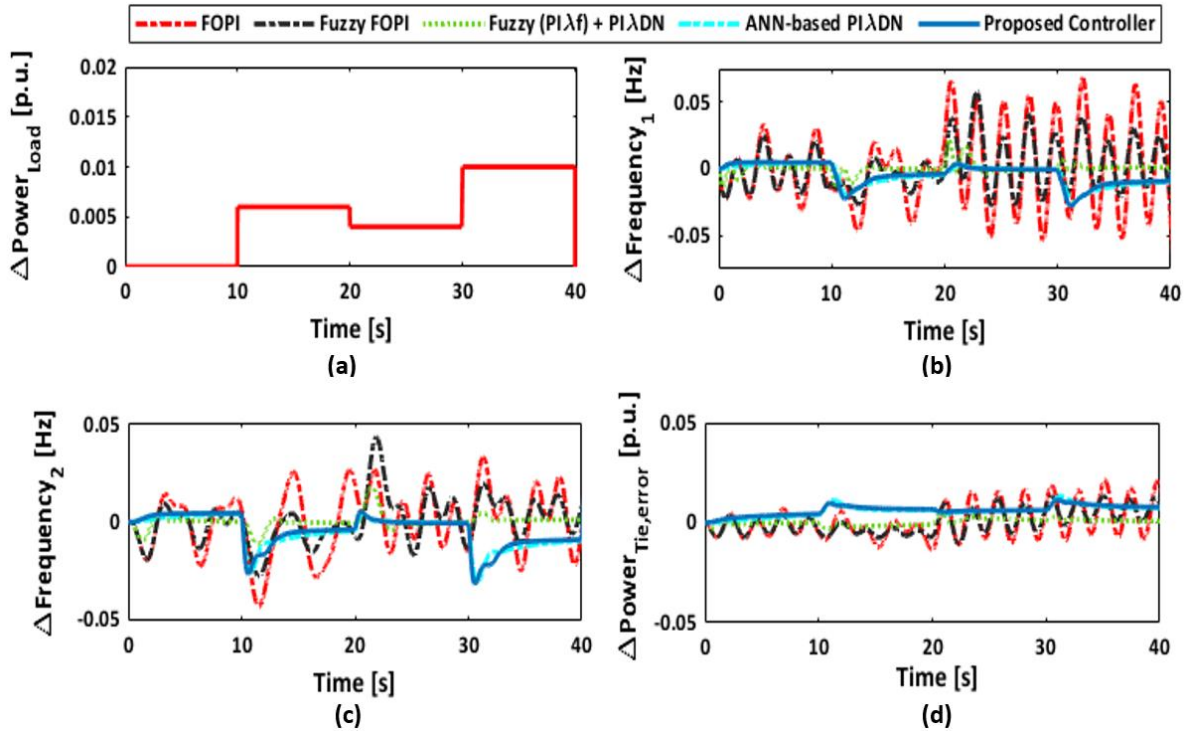

Fig. 12. RLD test system response to different controllers: a) random load pattern; b) area 1 frequency deviation; c) area 2-frequency deviation; d) tie-line power exchange deviation.

HVDC converters frequently include DC capacitors. These capacitors aid in frequency regulation. In this article, the authors examine how the presented test setup's LFC may change if the HVDC tie-line were modified to meet IET specifications. The thermal power system (GENCO-1) is in charge of seventy percent of the load shift in area 1, and the gas turbine system is in charge of the remaining thirty percent. (GENCO-2). Similar to this, 40% comes from hydropower and 60% from area 2 thermal power plants. Both sections consider the SLD of 0.01 p.u. in contrast to the initial case study. In this BBT case, DPM matrices can be written as an Eq. (20).

$$DPM = \begin{bmatrix} 0.2 & 0.1 & 0.2 & 0.1 \\ 0.4 & 0.3 & 0.4 & 0.3 \\ 0.3 & 0.2 & 0.2 & 0.1 \\ 0.1 & 0.4 & 0.2 & 0.5 \end{bmatrix} \quad (20)$$

Using an alternating current (AC) tie-line, Scenario 1 examines the proposed system's dynamic response. In case 2, a parallel HVDC tie-line based on AC-IET technology eventually replaces the AC tie-line. The research Table 5 displays the ideal control parameters. Fig. 13(a) and (b) show the frequency deviation response of the system for the two possible outcomes. Results demonstrate that the presence of an IET-based HVDC (High Voltage Direct Current) tie-line reduces undershoot by 59.30% and 49.78%, respectively. In Table 6, those numerical comparisons are displayed. The GENCOs' answer is shown in Fig. 13(c), and a similar scenario

is shown in Fig. 13(d). To determine Scenario 2's sensitivity to system parameter changes, the authors also perform a sensitivity analysis. The QOVPL-optimized stability of the suggested controller is tested by varying the input parameters by ±25% of their normal range. To perform sensitive studies, it is essential to know the power system gain (K_{PSi}), time constant (T_{PSi}), thermal turbine constant (T_{ti}), thermal governor time constant (T_{Gi}), transient droop (T_R & T_{RH}) parameters of the hydro system, and gas turbine parameters (X, Y, b_i, and c_i). The numerical study, tabulated in Table 7, demonstrates the robustness of the suggested controller.

6.2 Case Study 2: Contract Breach and a Review of Related Literature

DISCOs who break contracts frequently try to take advantage of their position for more significant reasons. The GENCOs present there would provide all of the emergency power needed in those areas. The section assumes that DISCOs in area 1 are requesting a 0.05 p.u. increase over the base rate (0.01 + 0.005). To meet client expectations, both GENCOs have altered production. The RES is activated in the 20s and continues to operate throughout the 40s, adding 0.005 p.u. to the simulation. After this time, conventional sources will again give the agreed-upon amount of power, and RES will have supplied any extra power required. Because the RES is unpredictable, it is anticipated that after the simulation's 40s, the generation will fall from 0.005 p.u. to 0.003 p.u.

Table 5. QOVPL's best gain values under various secenarios, both with and without an IET-based HVDC tie-line.

Control Parameters	Scenario-1		Scenario-2		Scenario-3		Scenario-4	
	A1	A2	A1	A2	A1	A2	A1	A2
K_{pi}	0.1131	0.2209	0.2665	0.0273	0.0690	0.2128	0.4006	0.3218
K_{Ii}	0.2845	0.2571	0.2403	0.1061	0.4002	0.3908	0.0811	0.5181
K_{Di}	0.0402	0.6450	0.0055	0.1530	0.0996	0.8251	0.0312	0.5943
K_{pfi}	0.8934	0.8603	0.8278	0.8144	0.8098	0.8024	0.8009	0.8002
K_{Ifi}	0.7639	0.7581	0.7404	0.7309	0.7263	0.7240	0.8114	0.8112
N_i	26.8547	20.6026	15.5680	44.0023	24.007	55.4318	32.3490	29.3467
λ_i	1.1156	1.1197	0.9744	0.8624	1.0017	1.0715	0.7861	0.6389
λ_{fi}	0.4123	0.4174	0.4028	0.4057	0.3998	0.3909	0.3901	0.3897
K_{1i}	0.9137	0.9082	0.8955	0.8734	0.8386	0.8347	0.8266	0.8230
K_{2i}	0.9366	0.9234	0.8940	0.8706	0.8345	0.8312	0.8238	0.8223
w_1	0.1958	0.2430	0.1023	0.2901	0.4855	0.3519	0.7994	0.8225
w_2	0.4583	0.7049	0.1402	0.5322	0.1228	0.1406	0.5930	0.3217

Table 6. Results of testing the effectiveness of hypotheses both with and without an IET-based HVDC tie-line.

Performance metric		Scenario 1	Scenario 2	Improvement [%]	Scenario 3	Scenario 4	Improvement [%]
OS	Δf_1	0.004004	0.00000	100	0.000319	0.000272	14.73
	Δf_2	0.00108	0.00000	100	0.000140	0.000121	13.57
US (-ve)	Δf_1	0.04917	0.02001	59.30	0.017205	0.01008	41.41
	Δf_2	0.052418	0.02632	49.78	0.010234	0.005167	4951
Ts	Δf_1	8.0918	8.0002	1.13	22.11	21.71	1.80
	Δf_2	9.5897	8.0975	15.56	23.71	23.02	2.91
OF		0.0208	0.0102	50.96	0.0033	0.0025	24.24

Table 7. Results of studying the system's sensitivity to significant input parameter changes.

Percent change in parameter		+25% of nominal			-25% of nominal		
Parameter		Ts	U.S (-ve)	O.S.	Ts	U.S (-ve)	O.S.
T_{G1}	Δf_1	14.3021	0.02005	0.0000	13.2364	0.02005	0.0000
	Δf_2	14.5631	0.02881	0.0000	13.6325	0.02880	0.0000
	$\Delta P_{tie,error}$	18.3455	0.00000	0.0281	18.3255	0.00000	0.0280
T_{G2}	Δf_1	14.5621	0.02005	0.0000	13.3554	0.02005	0.0000
	Δf_2	14.3437	0.02881	0.0000	13.6754	0.02881	0.0000
	$\Delta P_{tie,error}$	18.8457	0.00000	0.0283	18.6749	0.00000	0.0283
T_{t1}	Δf_1	14.9190	0.02005	0.0000	13.2835	0.02005	0.0000
	Δf_2	14.2633	0.02882	0.0000	13.3855	0.02882	0.0000
	$\Delta P_{tie,error}$	18.6731	0.00000	0.0283	18.6654	0.00000	0.0283
T_{t2}	Δf_1	14.4002	0.02004	0.0000	13.6652	0.02004	0.0000
	Δf_2	14.6790	0.02883	0.0000	13.5599	0.02881	0.0000
	$\Delta P_{tie,error}$	18.7836	0.00000	0.0284	18.2128	0.00000	0.0284
T_{RH}	Δf_1	14.4430	0.01988	0.0000	13.4457	0.01986	0.0000
	Δf_2	14.9056	0.02842	0.0000	13.7894	0.02822	0.0000
	$\Delta P_{tie,error}$	18.3658	0.00000	0.0283	18.6931	0.00000	0.0282
K_{PS1}	Δf_1	14.9235	0.02013	0.0000	13.3458	0.02013	0.0000
	Δf_2	14.2389	0.02944	0.0000	13.7840	0.02944	0.0000
	$\Delta P_{tie,error}$	18.7856	0.00000	0.0286	18.1128	0.00000	0.0287
T_{PS1}	Δf_1	14.2089	0.02034	0.0000	13.2785	0.02033	0.0000
	Δf_2	14.1141	0.02811	0.0000	13.5642	0.02811	0.0000
	$\Delta P_{tie,error}$	18.7867	0.00000	0.0284	18.6656	0.00000	0.0284
K_{PS2}	Δf_1	14.5634	0.02136	0.0000	13.6783	0.02135	0.0000
	Δf_2	14.4578	0.03046	0.0000	13.5560	0.03044	0.0000
	$\Delta P_{tie,error}$	18.5680	0.00000	0.0296	18.1348	0.00000	0.0296
T_{PS2}	Δf_1	14.5609	0.02014	0.0000	13.4599	0.02013	0.0000
	Δf_2	14.2118	0.02945	0.0000	13.4285	0.02944	0.0000
	$\Delta P_{tie,error}$	18.3478	0.00000	0.0285	18.4430	0.00000	0.0284
T_{GH}	Δf_1	14.0678	0.02039	0.0000	13.8657	0.02038	0.0000
	Δf_2	14.7728	0.02817	0.0000	13.1553	0.02816	0.0000
	$\Delta P_{tie,error}$	18.4678	0.00000	0.0286	18.4562	0.00000	0.0286
T_R	Δf_1	14.4781	0.02029	0.0000	13.5564	0.02028	0.0000
	Δf_2	14.4486	0.02928	0.0000	13.5125	0.02927	0.0000
	$\Delta P_{tie,error}$	18.3376	0.00000	0.0286	18.1780	0.00000	0.0285
c_g	Δf_1	14.8640	0.02152	0.0000	13.5673	0.02151	0.0000
	Δf_2	14.8865	0.02881	0.0000	13.5609	0.02880	0.0000
	$\Delta P_{tie,error}$	18.4458	0.00000	0.0287	18.3329	0.00000	0.0286
b_g	Δf_1	14.7890	0.02005	0.0000	13.5532	0.02004	0.0000
	Δf_2	14.8890	0.02871	0.0000	13.4479	0.02870	0.0000
	$\Delta P_{tie,error}$	18.9328	0.00000	0.0284	18.1783	0.00000	0.0283
X	Δf_1	14.7855	0.01954	0.0000	13.4329	0.01952	0.0000
	Δf_2	14.0945	0.02860	0.0000	13.7856	0.02858	0.0000
	$\Delta P_{tie,error}$	18.1178	0.00000	0.0283	18.1673	0.00000	0.0281
Y	Δf_1	14.6398	0.02089	0.0000	13.5673	0.02086	0.0000
	Δf_2	14.3212	0.02884	0.0000	13.4567	0.02882	0.0000
	$\Delta P_{tie,error}$	18.6682	0.00000	0.0286	18.7717	0.00000	0.0286

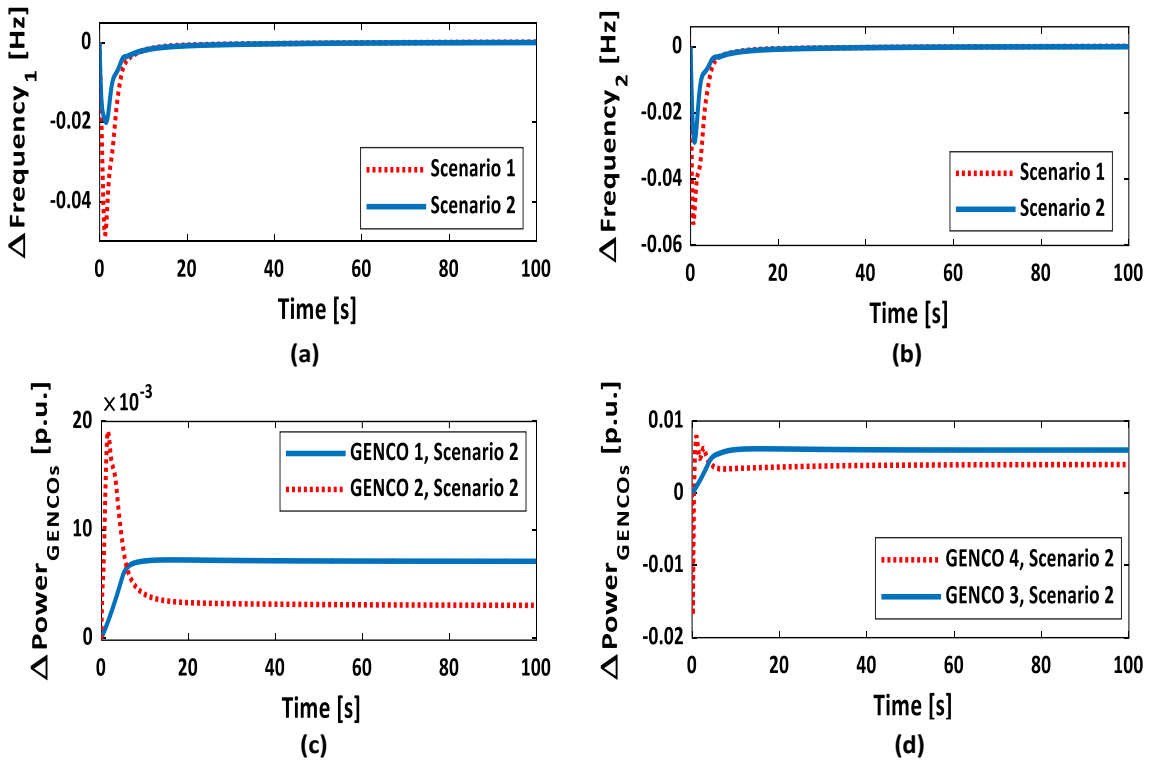

Fig. 13. BBT responses: a) frequency deviation in area 1 for scenarios 1 and 2; b) frequency deviation in area 2 for scenarios 1 and 2; c) the response from the GENCO in area 1; d) the response from the GENCO in area 2.

The remaining 0.002 p.u. over this period will be shared equally between GENCOs 1 and 2. The analysis is done for both possible outcomes, one with and one without the HVDC tie-line (Scenarios 3 and 4). However, compared to RES with intermittent output, the transient responsiveness of HVDC tie-lines based on IET is significantly better. Fig. 14 shows both the frequency response to this hypothetical situation and how the GENCOs would respond to it.

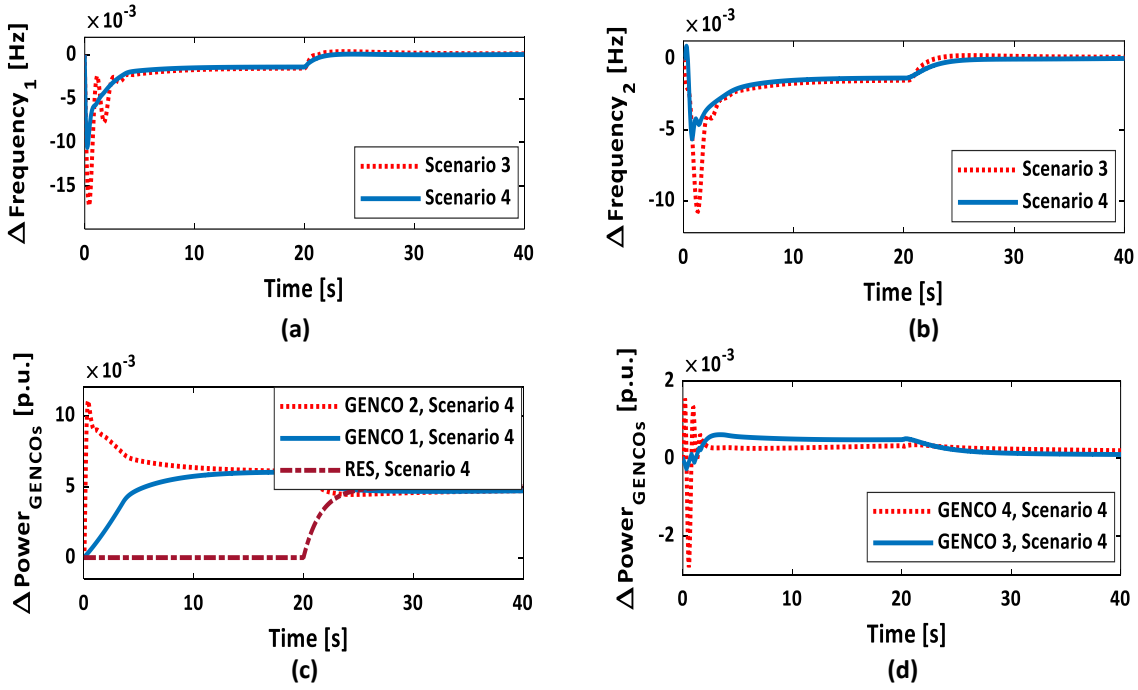

Fig. 14. Response of the tested system Contract Violation-based Transaction (CVT): a) area 1frequency deviation for scenarios 3 and 4;, b) area 2 frequency deviation for scenarios 3 and 4; c) area 1 GENCO response; d) area 2 GENCO response.

The ideal gains and numerical analysis for this scenario are shown in Tables 4 and 5, respectively. The effectiveness of the proposed QOVPL-optimized controllers based on ANN-based ($PI^{\lambda f}$ + $PI^{\lambda}DN$) is also judged by looking at what has been done before [25]. The authors employed a PIDF (1 + FOD) controller optimized by a salp swarm in their experiments. By switching to the proposed LFC technique from a salp swarm-optimized PIDF (1 + FOD) controller, the original frequency response of the system can be restored.

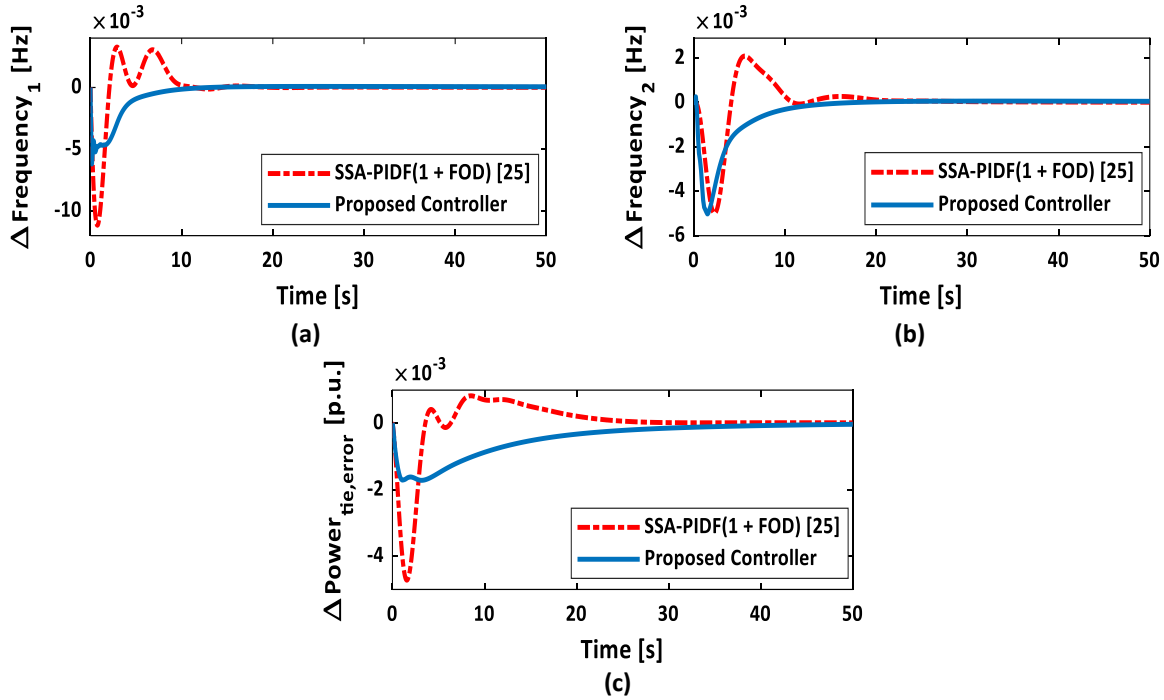

Fig. 15. Response of the test system shown in [25]: a) area 1 frequency deviation; b) area 2 frequency deviation; c) deviation in the tie-line power exchange.

The dynamic response of the system is depicted in Fig. 15. Table 8 displays the results of the numerical analysis used to prove the improved transient behavior produced by the suggested controller. This exhibits the proposed controller's flexibility for use with different kinds of testing apparatus. From the above results and discussions, a two-area thermal-hydro-gas power test system was modeled in a deregulated environment. The presence of an IET-based HVDC tie-line reduces undershoot by 59.30% (frequency in area 1, i.e., Δf1) and 49.78% (frequency in area 2, i.e., Δf2), respectively. The result reveals that the HVDC tie-line based on IET, on the other hand, does a fantastic job of maintaining the nominal values of the power system.

Table 8. Comparison between the proposed controller and the one reported in [25].

Performance metric		Ref. [25]	Proposed Controller	Improvement [%]
OS	Δf_1	0.0033	0.0025550	22.57
	Δf_2	0.0021	0.0018426	12.25
	ΔP_{12}	0.000829	0.0002432	70.66
US (-ve)	Δf_1	0.0112	0.0075448	32.63
	Δf_2	0.0050	0.0045501	8.99
	ΔP_{12}	0.0047	0.0019207	59.13
Ts	Δf_1	9.0973	8.5621	5.88
	Δf_2	16.8061	16.1012	4.19
	ΔP_{12}	19.2226	18.11932	5.73
OF		0.0002435	0.0001127	53.71

All key GENCOs are fully involved in the deregulated power system under the Poolco-Based Transactions (PBT), Bilateral-Based Transactions (BBT), and Contract Violation-based Transaction (CVT) scenarios. When SLD is taken into account, the proposed controller performs better than the majority of frequently used alternative settings.

7. CONCLUSIONS

This article delivers a novel control configuration for the proposed LFC scheme for the two-area power system with RES in the deregulated environment. The effect of the IET-based modified HVDC tie-line was analyzed for the tested system. The study used the efficient QOVPL technique to obtain the different parameters of the proposed controller through the ITAE performance index, considerably enhancing the controller's overall performance and system stability. A novel ANN-based ($PI^{\lambda f}$ + $PI^{\lambda}DN$) controller and robust overall precise control performance and consequence enhance the overall system stability of the tested system. The QOVPL approach creates optimal settings that can resist even random load disruptions. In this proposed work all possible scenario of deregulation i.e., PBT, BBT, and CVT has been validated. The proposed control scheme has also been validated and observed to improve performance by comparing the controller performance with recent published work. Because of the widespread adoption of electric vehicles, energy storage devices, and smart grid concepts, this research paper may be expanded in the future.

Appendix

Table A.1. System parameters.

System	Parameter	Value	Parameter	Value
Thermal	TGi	0.08	Gas: X	0.6
	Tti	0.3	Y	1.1
	Kri	0.5	cg	1
	Tri	10	bg	0.049
Hydro	TGH	0.2	TCR	0.01
	TR	5	TF	0.239
	TRH	28.75	TCD	0.2
	Tw	1	RES: TPV	1.5
	TWTS	1.8		
Power System	KPsi	120	RTH = RGT = RH	2.4
	TPSi	20	a12	-1/2
	For case 2:	apf11 = 0.7, apf12 = 0.3, apf21 = 0.6	ACE participation factors for case 1 and 3:	apf11 = apf12 = apf21 = apf22 = 0.5
	Bi	0.425	IET: SDC	600MW
	apf22	0.4	C	0.148mF
	VDC	300 KV	N	2
	H	4		

REFERENCES

[1] P. Kundur, *Power System Stability and Control,* McGraw-Hill, New York, 1994.

[2] P. Kumar, D. Kothari, "Recent philosophies of automatic generation control strategies in power systems," *IEEE Transactions on Power Systems,* vol. 20, no. 1, pp. 346-357, 2005, doi: 10.1109/TPWRS.2004.840438.

[3] M. Ranjan, R. Shankar, "A literature survey on load frequency control considering renewable energy integration in power system: recent trends and future prospects," *Journal of Energy Storage,* vol. 45, p. 103717, 2022, doi: 10.1016/j.est.2021.103717.

[4] A. Saxena, R. Shankar, "Improved load frequency control considering dynamic demand regulated power system integrating renewable sources and hybrid energy storage system," *Sustainable Energy Technologies and Assessments,* vol. 52, p. 102245, 2022, doi: 10.1016/j.seta.2022.102245.

[5] A. Saxena, R. Shankar, S. Parida, R. Kumar, "Demand response based optimally enhanced linear active disturbance rejection controller for frequency regulation in smart grid environment," *IEEE Transactions on Industry Applications,* vol. 58, no. 4, pp. 4337-4349, 2022, doi: 10.1109/TIA.2022.3166711.

[6] P. Aryan, G. Raja, "Design and analysis of novel QOEO optimized parallel fuzzy FOPI-PIDN controller for restructured AGC with HVDC and PEV," *Iranian Journal of Science and Technology, Transactions of Electrical Engineering,* vol. 46, pp. 565-587, 2022, doi: 10.1007/s40998-022-00484-7.

[7] M. Ranjan, R. Shankar, "A cascade fractional type-II fuzzy control approach for enhancing frequency stability in a smart grid system with diverse energy resources," *Iranian Journal of Science and Technology, Transactions of Electrical Engineering,* vol. 47, pp. 1537-1560, 2023, doi: 10.1007/s40998-023-00642-5.

[8] P. Vidyarthi, A. Kumar, "A modified tilt controller for AGC in hybrid power system integrating forecasting of renewable energy sources," *Optimal Control Applications and Methods,* vol. 45, no. 1, pp. 1–23, 2023, doi:10.1002/oca.3052.

[9] D. Guha, P. Roy, S. Banerjee, "Quasi-oppositional backtracking search algorithm to solve load frequency control problem of interconnected power system," *Transactions of Electrical Engineering,* vol. 44, no. 2, pp. 781–804, 2020, doi: 10.1007/s40998-019-00260-0.

[10] M. Khamies, G. Magdy, M. Ebeed, S. Kamel, "A robust PID controller based on linear quadratic Gaussian approach for improving frequency stability of power systems considering renewables," *ISA Transactions,* vol. 117, pp. 118-138, 2021, doi: 10.1016/j.isatra.2021.01.052.

[11] M. Ahmed, G. Magdy, M. Khamies, S. Kamel, "Modified TID controller for load frequency control of a two-area interconnected diverse-unit power system," *Electrical Power and Energy Systems,* vol. 135, p. 107528, 2022, doi: 10.1016/j.ijepes.2021.107528.

[12] Y. Arya, "A novel CFFOPI-FOPID controller for AGC performance enhancement of single and multi-area electric power systems," *ISA Transactions,* vol. 100, pp. 126–135, 2020, doi: 10.1016/j.isatra.2019.11.025.

[13] K. Singh, M. Amir, Y. Arya, "Optimal dynamic frequency regulation of renewable energy based hybrid power system utilizing a novel TDF-TIDF controller," *Energy Sources, Part A: Recovery, Utilization, and Environmental Effects,* vol. 44, no. 4, pp. 10733–10754, 2022, doi: 10.1080/15567036.2022.2158251.

[14] A. Saxena, R. Shankar, O. Zaabi, K. Hosani, U. Muduli, "Rule-based adaptive frequency regulation with real stochastic model intermittency in a restructured power system," *IEEE Transactions on Industrial Informatics,* vol. 20, no. 2, pp. 2907-2919, 2023, doi: 10.1109/TII.2023.3299422.

[15] N. Patel, B. Sahu, "Design and implementation of a novel FO-hPID-FPID controller for AGC of multi-area interconnected nonlinear thermal power system," *International Transactions on Electrical Energy Systems,* vol. 31, no. 11, p. 13078, 2021, doi: 10.1002/2050-7038.13078.

[16] U. Raj, R. Shankar, "Optimally enhanced fractional-order cascaded integral derivative tilt controller for improved load frequency control incorporating renewable energy sources and electric vehicle," *Soft Computing,* vol. 27, pp. 15247–15267, 2023, doi: 10.1007/s00500-023-07933-3.

[17] S. Murali, R. Shankar, "Exploration of novel optimal fuzzy-based controller for enhancement of frequency regulation of deregulated hybrid power system with modified HVDC tie-line," *International Journal of Intelligent Systems,* vol. 37, no. 7, pp. 4163-4189, 2022, doi: 10.1002/int.22715.

[18] L. Jin, C. Zhang, X. Shangguan, L. Jiang, M. Wu, "Robust delay-dependent load frequency control of wind power system based on a novel reconstructed model," *IEEE Transactions on cybernetics,* vol. 52, no. 8, pp. 7825-7836, 2022, doi: 10.1109/TCYB.2021.3051160.

[19] P. Sharma, A. Mishra, A. Saxena, R. Shankar, "A novel hybridized fuzzy PI-LADRC based improved frequency regulation for restructured power system integrating renewable energy and electric vehicles," *IEEE Access,* vol. 9, pp. 7597–7617, 2021, doi: 10.1109/ACCESS.2020.3049049.

[20] A. Jawahar, K. Ramakrishnan, "Impact of time delay margin on the stability of load frequency systems with electric vehicle aggregator," *Jordan Journal of Electrical Engineering,* vol. 8, no. 2, pp. 151-164, 2022, doi: 10.5455/jjee.204-1636958206.

[21] D. Dinakin, P. Oluseyi, "Optimal under-frequency load curtailment via continuous load control in a single area power system using fuzzy logic, PID fuzzy and neuro fuzzy (ANFIS) controllers," *Jordan Journal of Electrical Engineering,* vol. 4, no. 4, pp. 208-223, 2018.

[22] A. Anand, P. Aryan, N. Kumari, G. Raja, "Type-2 fuzzy-based branched controller tuned using arithmetic optimizer for load frequency control," *Energy Sources, Part A: Recovery, Utilization, and Environmental Effects,* vol. 44, no. 2, pp. 4575–4596, 2022, doi: 10.1080/15567036.2022.2078444.

[23] S. Murali, R. Shankar, "Assessment of amelioration in frequency regulation by deploying novel intelligent based controller with modified HVDC tie-line in deregulated environment," *Smart Science,* vol. 11, no. 1, pp. 154-170, 2022, doi: 10.1080/23080477.2022.2054197.

[24] K. Manoj, R. Agrawal, S. Tripathy, S. Choudhury, "Artificial neural network tuned PID controller for LFC investigation including distributed generation," *International Journal of Numerical Modelling Electronic Network, Devices and Fields,* vol. 35, no. 5, p. 2740, 2020, doi: 10.1002/jnm.2740.

[25] A. Prakash, K. Kumar, S. Parida, "PIDF (1 + FOD) controller for load frequency control with SSSC and AC – DC tie-line in deregulated environment," *IET Generation, Transmission & Distribution,* vol. 14, no. 14, pp. 2751–2762, 2020., doi: 10.1049/iet-gtd.2019.1418.